

See discussions, stats, and author profiles for this publication at: <https://www.researchgate.net/publication/304568185>

Estimation of coupling along the Main Himalayan Thrust in the Central Himalaya

Article · June 2016

DOI: 10.1016/j.jseaes.2016.05.028

CITATIONS

0

READS

109

5 authors, including:



François Jouanne

Université Savoie Mont Blanc

82 PUBLICATIONS 1,111 CITATIONS

[SEE PROFILE](#)



Jean-Louis Mugnier

CNRS

126 PUBLICATIONS 2,231 CITATIONS

[SEE PROFILE](#)



Arnaud Pêcher

University Joseph Fourier - Grenoble 1

116 PUBLICATIONS 3,747 CITATIONS

[SEE PROFILE](#)

Some of the authors of this publication are also working on these related projects:



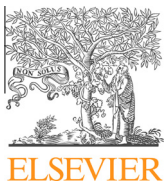
Gestión integral del riesgo en las regiones costeras de Venezuela, con énfasis en la amenaza por tsunami [View project](#)



HP-UHP in Himalaya [View project](#)

All content following this page was uploaded by [François Jouanne](#) on 08 July 2016.

The user has requested enhancement of the downloaded file. All in-text references [underlined in blue](#) are added to the original document and are linked to publications on ResearchGate, letting you access and read them immediately.



Contents lists available at ScienceDirect

Journal of Asian Earth Sciences

journal homepage: www.elsevier.com/locate/jseas

Full length Article

Estimation of coupling along the Main Himalayan Thrust in the central Himalaya

François Jouanne ^{a,b,*}, Jean Louis Mugnier ^{a,b}, Som Nath Sapkota ^c, Pascale Bascou ^{a,b}, Arnaud Pecher ^{d,b}^a Université Savoie Mont Blanc, ISTerre, F-73376 Le Bourget du Lac, France^b CNRS, ISTerre, F-38058 Grenoble, France^c Department of Mines and Geology, Lainchaur, Kathmandu, Nepal^d Univ. Grenoble Alpes, ISTerre, F-38058 Grenoble, France

ARTICLE INFO

Article history:

Received 31 December 2015

Received in revised form 10 May 2016

Accepted 27 May 2016

Available online xxxx

Keywords:

Himalaya

GPS

Main Himalayan Thrust

Coupling

Nepal

Gorkha earthquake

ABSTRACT

We analyze episodic (1995–2010) and permanent GNSS data quantifying interseismic velocities in the Himalaya of Nepal so as to constrain spatial variations in coupling along the Main Himalayan Thrust. To estimate this coupling, we model the MHT with the help of cross sections allowing us to constrain its changes in geometry from far-western Nepal to central and eastern Nepal. We determine that the upper flat of the MHT is nearly totally locked, the crustal ramp is partially locked, and that free slip is localized only along the lower flat north of the Himalaya. This location of increased coupling probably corresponds to the brittle/ductile change in rheology along the MHT and explains the location of very large (greater than the Gorkha 2015 event) earthquake epicenters north of the crustal ramp. Including the simulation of the Western Nepal Fault System in the continuation of the Karakorum fault does not improve simulation of the interseismic velocity field. The 25 April Gorkha earthquake nucleated in a highly coupled part of the upper flat of the MHT and propagated eastward along a less coupled part of the MHT.

© 2016 Elsevier Ltd. All rights reserved.

1. Introduction

The structure of the Himalaya results from underthrusting of the Indian lithosphere along the Main Himalayan Thrust (MHT) beneath the Tibetan Plateau (Argand, 1924; Zhao et al., 1993). Great earthquakes have episodically ruptured segments of the brittle upper part of the MHT (e.g. Chandra, 1992; Avouac et al., 2001; Mugnier et al., 2011). It is inferred that the great earthquakes such as the 1934 Bihar Nepal earthquake, the 1505 western Nepal earthquake, and the huge 1100 earthquake all initiated at the brittle/ductile transition (e.g. Avouac et al., 2001) and propagated along the crustal ramp and upper flat segments of the MHT (e.g. Schelling and Arita, 1991). During these large magnitude earthquakes, coseismic slip reached the surface along the Main Frontal Thrust (MFT) and can be observed in trenches (e.g. Kumar et al., 2006; Sapkota et al., 2013; Bollinger et al., 2014). Intermediate magnitude earthquakes such as the 1833 and 2015 (7.9 Mw) Gorkha earthquakes affect only a part of the brittle segment of the MHT. For example, the rupture of the 2015 Gorkha earthquake

did not reach the surface and affected neither the crustal ramp nor the shallower, southern part of the MHT (Galetzka et al., 2015; Grandin et al., 2015). In other cases, intermediate earthquakes, such as the out-of-sequence 2005 (Mw 7.6) Balakot-Bagh earthquake in the western Himalaya, affect only the crustal ramp where it connects the MHT to the surface (see Table 1).

To quantify present-day velocities during interseismic periods and coupling along the MHT as characterized by lateral variations in geometry, we analyzed episodic and permanent GNSS data (Fig. 1). These velocities have been modeled using sets of dislocations describing the upper flat of the MHT, the crustal ramp with its east–west lateral variations as documented by cross sections, and the lower flat that allows the underthrusting of the Himalaya beneath Tibet (Fig. 2; Mugnier et al., 2013). Vertical velocities obtained from leveling comparison (Jackson and Bilham, 1994) have been used.

2. Data analysis

In order to monitor and determine present-day velocities in the Himalaya, an episodic GPS network was established in 1995 and measured again in 1997, 1998, 2000, and 2010 as part of an Isterre-DMG cooperation program (Fig. 1). This network, which

* Corresponding author at: Université Savoie Mont Blanc, ISTerre, F-73376 Le Bourget du Lac, France.

E-mail address: fjoua@univ-savoie.fr (F. Jouanne).

Table 1

Time occupation of episodic GPS points.

	1995	1997	1998a	1998b	2000	2003	2004	2010
AMPO	3 * 12 h		4 * 24 h		4 * 24 h			4 * 24 h
BALO	2 * 12 h		3 * 24 h					
BBPO	3 * 12 h		4 * 24 h					
BCHO	3 * 12 h		4 * 24 h					
BMT0	3 * 12 h		3 * 24 h		4 * 24 h			
CHIO	3 * 12 h		2 * 24 h					
CHPO	5 * 12 h	5 * 24 h						
CHU0	6 * 12	2 * 24 h						
DAD2			3 * 24 h		5 * 24 h			3 * 24 h
DDLO			3 * 24 h		3 * 24 h			2 * 24 h
DLPO	3 * 12 h		4 * 24 h					1 * 24 h
DMNO	4 * 12 h		2 * 24 h					
GMB0	2 * 12 h		2 * 24 h					
GURO	3 * 12 h	3 * 24 h	3 * 24 h					5 * 24 h
GUTO	3 * 12 h		4 * 24 h					4 * 24 h
HETO	2 * 12 h		3 * 24 h					
JOM0	12 * 24 h		4 * 24 h		4 * 24 h			3 * 24 h
KKNO	5 * 12 h		12 * 24 h					
KRN2			2 * 24 h		6 * 24 h			4 * 24 h
KUS1	1 * 12 h	4 * 24 h	3 * 24 h		4 * 24 h			
MAHO	2 * 12 h	4 * 24 h	4 * 24 h		12 * 24 h			3 * 24 h
MULO	3 * 12 h	3 * 24 h	4 * 24 h					4 * 24 h
NIJO	2 * 12 h				3 * 24 h			
NPJO	8 * 12 h	17 * 24 h	7 * 24 h		5 * 24 h			3 * 24 h
PKIO	8 * 12 h		13 * 24 h					
PKRO	1 * 12 h		8 * 24 h		3 * 24 h	13 * 24 h		
POKO	4 * 12 h		1 * 24 h		2 * 24 h			
RAM0	2 * 12 h		2 * 24 h					
SHBO	3 * 24 h	5 * 24 h	4 * 24 h		5 * 24 h			
SHPO	1 * 24 h	4 * 24 h	3 * 24 h		4 * 24 h			6 * 24 h
SKAO		16 * 24 h			10 * 24 h			
SKTO	10 * 24 h				3 * 24 h			
SMKO	13 * 24 h	5 * 24 h	4 * 24 h					1 * 24 h
SYAO	3 * 24 h		3 * 24 h					
TANO	6 * 12 h		4 * 24 h		4 * 24 h		3 * 24 h	4 * 24 h
KUSU			1 * 24 h		4 * 24 h			5 * 24 h
JALT			4 * 24 h		7 * 24 h			6 * 24 h
GANS			3 * 24 h		6 * 24 h			7 * 24 h
TUKO			3 * 24 h		4 * 24 h			4 * 24 h

shared points with the Cires network, has been supplemented by the LDG-DASE episodic GPS network established in central Nepal. Episodic measurements were made in 12-h long sessions in 1995 and 24-h long sessions during the other campaigns. This network was supplemented by continuous GNSS networks established by LDG-DASE, Caltech (www.unavco.org) and by Central Washington University (<http://www.geodesy.cwu.edu>); data from the installation of permanent GNSS stations to the day before the 25 April earthquake were analyzed to constrain horizontal velocities and also the vertical component of velocities. Data were analyzed using Bernese 5.2 software, with absolute antenna phase center offset models, together with precise orbits and earth rotation parameters recomputed in the IGB08 reference frame by the Center for Orbit Determination for Europe (CODE), which allows for orbits in the same reference frame from the first measurements in 1995 until the present day. Velocities (Table 2) were estimated in the IGB08 frame of reference (an IGS-specific realization of ITRF2008) with discontinuities associated with this reference frame and expressed in terms of the India fixed reference frame by the use of a rotation pole as proposed by [Ader et al. \(2012\)](#).

We followed the resolution strategy with (1) initial ionosphere-free analysis with computation of residuals; (2) residuals analysis; (3) code-based widelane ambiguity resolution for all the baselines ([Melbourne, 1985](#); [Wübbena, 1985](#)), using differential code bias (DCB) files when available and computation of the ionosphere-free solution with the introduction of the resolved Melbourne-Wübbena linear combination ambiguities; (4) phase-based wide-lane (L5) ambiguity resolution for baselines <200 km and computa-

tion of the ionosphere-free solution with the introduction of resolved ambiguities; (5) resolution of the previously unresolved ambiguities for baselines <2000 km using the quasi ionosphere-free strategy of resolution; (6) direct L1/L2 ambiguity resolution for baselines <20 km with the introduction of an ionosphere model; (7) computation of the normal equations; and (8) transformation of daily normal equations in the IGB08 reference frame with a six-parameter Helmert solution (three translation parameters and three rotation parameters) using the IGB08 stations. These normal equations were analyzed together to determine accurate velocities in the IGB08 reference frame with the introduction of IGB08 coordinates, velocities, and discontinuities. Outliers and new discontinuities were detected using the “Find Outliers and Discontinuities in Time Series” tool in the Bernese 5.2 software that reduces, step by step, the discrepancy between the functional model and the time series from statistical adjustment ([Ostini et al., 2008](#)) taking in annual and semi-annual seasonal fluctuations. As Bernese 5.2 software underestimates the daily errors because systematic errors or mismodeled parameters are not included in the formal error ([Hugentobler et al., 2001](#)), we rescaled the formal errors multiplying by a factor of 10 to obtain a more realistic estimated error.

GPS time series of permanent GNSS stations present seasonal variations probably associated with the loading of the Ganga plain during the monsoon and its unloading during the dry season ([Bettinelli et al., 2008](#); [Fu and Freymueller, 2012](#)). However, it should be emphasized that these times series allow us to exclude the occurrence of a detectable slow slip event along the brittle MHT during the years covered by the data acquisition.

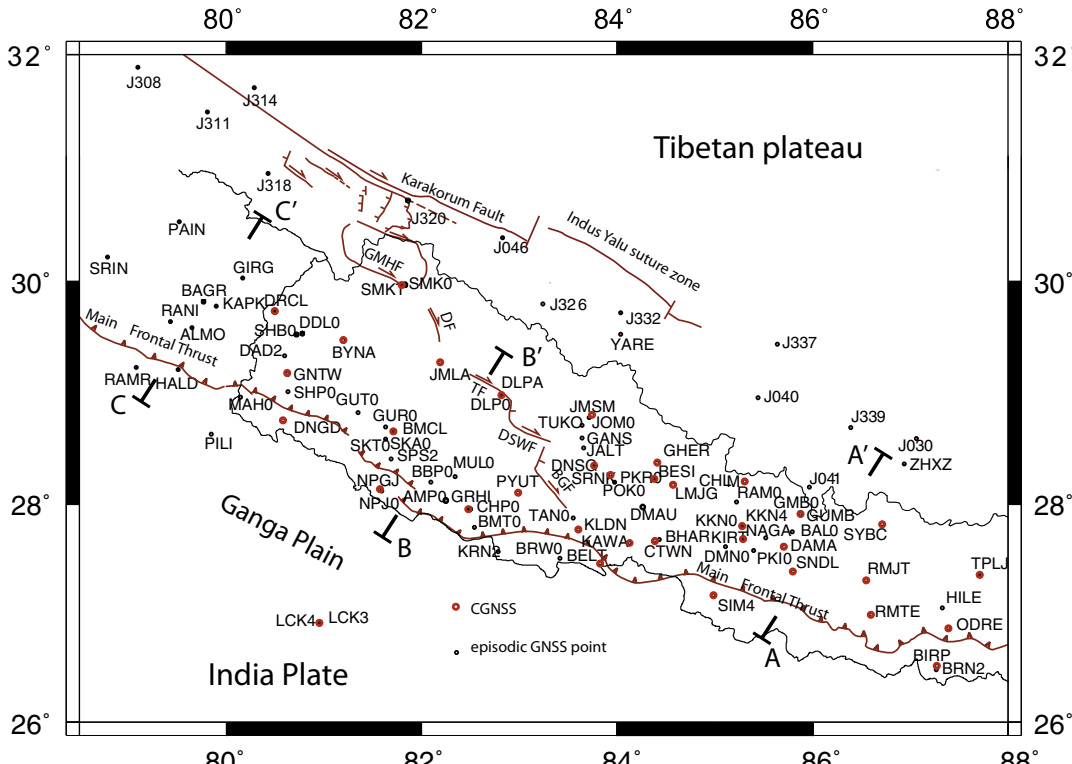


Fig. 1. Structural scheme of the Himalaya of Nepal and location of GNSS points (episodic and continuous GNSS measurements) and locations of crustal cross sections. GMH - Gurla Mandata-Humla fault; DF - Darma fault; TF - Tibrikot fault; DSWF - Dhaulagiri southwest fault; BGF - Bari Gad fault.

3. Results

In Fig. 3, we can observe the lack of significant velocities in the India fixed reference frame for points located in the Ganga plain and the lack of relative velocities between points located on either side of the Main Frontal Thrust, which is the emergent part of the Main Himalayan Thrust, to which most geological displacement along the MHT is transferred during large Himalayan earthquakes. We can conclude, then, that there is no significant creep along the MFT. Nevertheless, a velocity gradient can be observed across the Himalaya with southward velocities reaching 14 mm/year. Like many authors (Bilham et al., 1997; Jouanne et al., 1999, 2004; Berger et al., 2004; Bettinelli et al., 2006; Ader et al., 2012) we interpret this velocity gradient as the result of slip change along the MHT; ductile slip is localized along the lower ductile part of the MHT whereas its upper brittle part remains totally or partially locked during interseismic periods.

Vertical velocities (Fig. 4) deduced from CGNSS measurements and from leveling comparison (Jackson and Bilham, 1994) reveal an uplift gradient extending from the Ganga plain, which is characterized by zero vertical velocities, to the upper chain of Himalaya, where uplift reaches 8 mm/year. This uplift of the upper chain (Fig. 4) may reflect interseismic deformation but also a degree of glacial isostatic adjustment induced by the melting of the Himalayan glaciers (Shrestha and Aryal, 2011) in relation with the present-day global warming as has been illustrated in Iceland for example (Pagli et al., 2007).

4. Modeling

To model instantaneous horizontal velocities measured by GNSS and vertical velocities derived from leveling comparison (Jackson and Bilham, 1994) and permanent GNSS stations, we

assumed that the velocity field reflects slip distribution along the Main Himalayan Thrust, the fault that allows the Indian plate to underthrust and along which the large Himalayan earthquakes occur. For modeling we used our velocity field supplemented by a selection of velocities for Tibet (Liang et al., 2013) and India (Banerjee et al., 2008) (Fig. 3), and uplift rates constrained by leveling comparison (Jackson and Bilham, 1994) in order to better constrain slip distribution along the MHT (Fig. 4). As for these two data sets, the Ganga plain is characterized by null velocities, we suppose that we can use together these two data sets. We have considered the standard deviations of vertical velocities obtained by leveling comparison as given by Jackson and Bilham (1994) and for vertical velocities obtained by CGNSS measurements, we have considered standard deviations as estimated with the daily solutions combination. We have decided to not take into account vertical velocities of points located in the Katmandu valley because of the active subsidence of this area induced by the thick quaternary infill of this paleolake.

We assumed that the instantaneous deformation revealed by the velocity field can be simulated by a set of dislocations located in a uniform elastic half-space (Okada, 1985). We used the three cross sections of Fig. 2 to describe the flat-ramp-flat geometry of the MHT and its variations between far-western, western, and central-eastern Nepal (Mugnier et al., 2013). These cross-sections are a synthesis of geology and geophysics data or results of kinematic and thermal modeling. Nonetheless, they are still weakly constrained and errors of 50% are not excluded on the dip values. Recent receiver function data published by Duputel et al. (2016) showing a MHT geometry characterized by a southern large flat (95–100 km), a crustal ramp dipping 30° northward between 15 and 25 km and a northern flat are in very good accordance with the cross section describing the MHT geometry at the longitude of Katmandu.

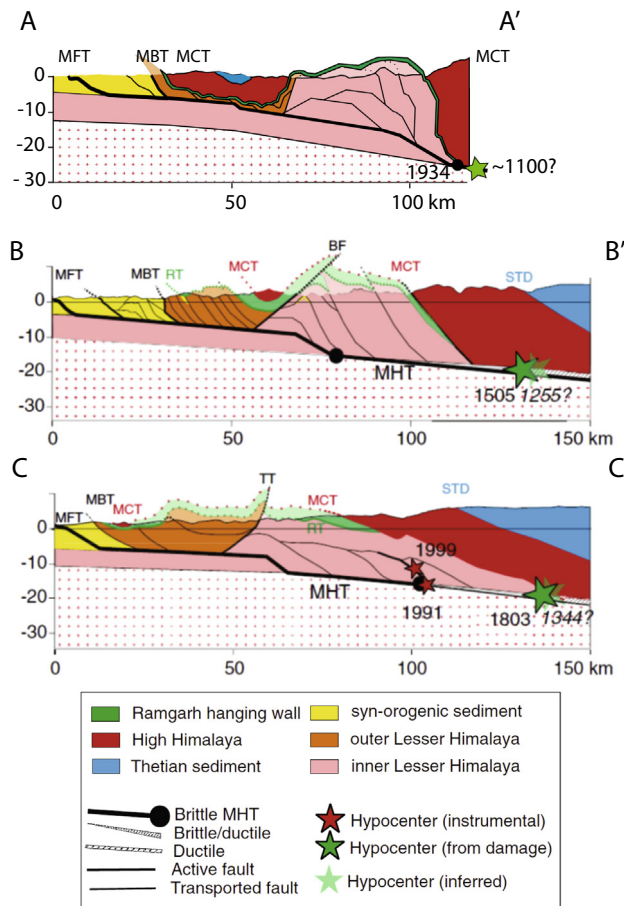


Fig. 2. Crustal cross sections across the Himalaya of Nepal illustrating the geometry changes of the Main Himalayan Thrust and locations of epicenters of large earthquakes. MCT: Main Central Thrust; MBT: Main Boundary Thrust; RT: Ramgarh Thrust; MFT: Main Frontal Thrust; STD: South Tibetan Detachment; TT: Tons Thrust; BF: Bhari Ghat fault; TKT: Tamur Khola Thrust.

In far-western Nepal, the MHT is characterized by a 60 km-wide upper flat with 3° dip and a narrow 6 km-wide crinal ramp with a dip of 54°. The lower flat, north of this small crinal ramp, has a 10° dip in our model.

In western Nepal the MHT is characterized by a 68 km-wide upper flat with 5° dip and a narrow 10 km-wide crinal ramp with a dip of 37°. The lower flat, north of this small crinal ramp, has a 10° dip in our model.

In central and eastern Nepal the MHT is characterized by a 100 km-wide upper flat with a 7° dip and a 22 km-wide crinal ramp with a dip of 28° as also shown by receiver functions analysis (Duputel et al., 2016). The lower flat, north of this crinal ramp, has a 10° dip in our model. The existence of this broad crinal ramp, the currently active thrust of a duplex located north of Katmandu, explains the existence of the high elevations east of Dhaulagiri, and the substantial changes in mean elevation and downcutting between western and central Nepal (Berger et al., 2004).

The MHT is represented by ~15 * 15 km rectangles for the upper flat and by ~5 * 5 km rectangles for the crinal ramps separating the upper and the lower flats in order to detect any coupling variations along the crinal ramp. The lower flat is described by ~20 * 20 km rectangles. Unlike Ader et al. (2012) and Stevens and Avouac (2015), we do not adopt a back-slip approach as this is only suitable for planar faults (Vergne et al., 2001). Instead we invert the slip components (dip-slip and strike-slip) directly on the patches describing the MHT.

During the inversion with sdm2011 software (Wang et al., 2009, 2011, 2012) we allow a slip rate up to 20 mm/year, the Quaternary slip rates along the MFT, i.e. the emergent part of the MHT (Lavé and Avouac, 2000; Mugnier et al., 2004); we also allow for a strike-slip component with rake varying from -110° to -50°. To compute coupling coefficient we have used 20 mm/year, the quaternary slip rate along the MHT, as reference value. We use a low, 0.2, smoothing factor in order to detect small scale variations in slip and then coupling variations that may reflect the existence of asperities along the MHT that can explain the location and the size of Himalayan earthquakes and particularly the characteristics of the 25 April 2015 Gorkha earthquake (Fig. 5 or 8 if the WNFS is added in the inversion). We have tested the influence of vertical velocities with model considering as input horizontal and vertical velocities and model considering as input only horizontal velocities. The data-model correlation with vertical velocities is 0.9905 whereas data model correlation without vertical velocities is 0.9898, we can then conclude that there is no significant changes between these two models. We have then decided to consider as adopted models, models obtained with vertical velocities as input.

To compare these models with a simpler geometry of the MHT, we have performed a test considering a flat MHT represented by ~15 * 15 km rectangles, without crustal ramp, with a 7° dip northward (Figs. 11–13).

5. Discussion

As clearly shown by residuals on horizontal and vertical components obtained for the flat MHT hypothesis (Figs. 12 and 13), and residuals obtained with models with a more realistic geometry (Figs. 6, 7, 9 and 10), data are better explained with models considering the existence of crustal ramps than with a model considering a flat geometry. We can particularly observe that uplift rates cannot be well simulated using the flat geometry model (Figs. 13, 7 and 10). Nevertheless, the coupling map is not so different compared to coupling maps obtained with a more realistic geometry of the MHT with a nearly fully locked southern part of the MHT and a northern part affected by a free slip (0 coupling).

As shown in Figs. 6 and 7 good simulations can be made using GPS velocities and uplift rates derived from leveling comparison across central Nepal and permanent GPS stations. Simulations for the high chain of the Himalaya predict local uplift rates reaching 7 mm/year (Fig. 14) less than the 8 mm/year maximum observed uplift. This discrepancy may reflect a dip of the crinal ramp greater than 30°, but this hypothesis is improbable as shown by the receiver functions analysis (Duputel et al., 2016) that allows to image, at the longitude of Katmandu, a nearly horizontal southern part of the MHT, a 25–30° crinal ramp and a nearly horizontal northern flat. Vertical velocities misfits may then reflect ongoing glacial isostatic adjustment induced by the current melting of the Himalayan glaciers (Shrestha and Aryal, 2011) as observed in other parts of the world (Pagli et al., 2007), erosion-induced strain and uplift as suggested for example by Vernant et al. (2013) for the western Alps where uplift rates up to 2 mm/year are observed whereas horizontal velocities are only a few tenths of mm/year.

Maximum free slip, with an absence of coupling, is found north of the MHT crinal ramp, which suggests (cf. Berger et al., 2004) that the progressive coupling along the MHT is due to a progressive change, probably a progressive ductile/brittle rheological change (Berger et al., 2004). This spatial evolution, the coupling changes from 1 to 0 in a distance between 30 and 60 km, reflects the progressive increase in temperature and pressure northward along the MHT. This behavior is consistent with the hypothesis that large Himalayan earthquakes nucleate north of the crinal ramp and propagate southward to reach the MFT 120 km south of the crinal

Table 2

Velocities expressed in the India fixed reference frame.

Site	Longitude	Latitude	ν_e	σ_e	ν_n	σ_n	ν_{up}	σ_{up}
MAHO	80.148	28.9632	-0.77	0.1	0.31	0.1		
DRCL AA	80.5009	29.7338	-4.78	0.1	-5.36	0.1		
DRCL	80.5009	29.7338	-3.51	0.1	-4.21	0.1	4.26	0.2
DNGD	80.5818	28.7544	1.16	0.01	0.9	0.01	-0.46	0.1
DAD2	80.6019	29.3342	-1.23	0.1	-0.9	0.1		
GNTW	80.6262	29.1765	-4.2	0.1	0.04	0.1		
SHPO	80.6364	29.0124	-0.98	0.1	-0.22	0.1		
SHBO	80.7214	29.5267	-2.52	0.4	-6.51	0.4		
DDL0	80.7798	29.5347	-2.84	0.2	-4.22	0.2		
LCK4	80.9556	26.9121	-3.87	0.8	0.22	0.7	-0.85	0.3
LCK3	80.9556	26.9122	-5.47	0.8	-0.24	0.7	-1.34	0.3
LCK1 22305M002	80.9559	26.9124	-0.17	0.1	-0.2	0.1		
LCK2 22305M003	80.956	26.9126	0.01	0.1	-0.38	0.1		
BYNA	81.2007	29.4742	-3.54	0.1	-7.22	0.1	5.19	0.2
GUTO	81.3532	28.8237	-0.94	0.1	-0.89	0.01		
NPJO	81.5747	28.1341	-0.29	0.1	-0.22	0.1		
NPGJ	81.5953	28.1172	-0.8	0.01	1.63	0.01	0.58	0.1
GURO	81.6299	28.6971	-1.34	0.1	-1.36	0.1		
SKAO	81.6343	28.5829	-1.35	0.2	-2.32	0.3		
SKTO	81.6352	28.5858	0.15	0.4	-1.79	0.4		
SPS2	81.6906	28.4069	-0.23	0.7	-2.76	0.7		
BMCL AA	81.7144	28.6558	-1.98	0.1	-0.7	0.1		
BMCL	81.7144	28.6558	-1.87	0.1	-1.82	0.1	1.31	0.2
SMKT	81.8065	29.9694	-4.04	0.1	-12.34	0.01	4.99	0.1
SMKO	81.8265	29.967	-2.79	0.1	-12.45	0.01		
BBPO	82.0937	28.1957	4.92	0.8	-0.02	0.8		
JMLA	82.1926	29.2778	-3.68	0.01	-8.46	0.01	3.96	0.1
AMPO	82.2474	28.0297	-0.96	0.1	-0.11	0.1		
MULO	82.3465	28.2494	-0.71	0.1	-0.41	0.1		
GRHI	82.4912	27.9508	-0.87	0.01	-0.46	0.01	1.63	0.1
CHPO	82.5042	27.9509	1.72	1	-0.91	0.9		
BMT0	82.5398	27.7857	-0.37	0.5	-0.08	0.4		
KRN2	82.7848	27.5678	-0.07	0.1	0.95	0.1		
DLPO	82.8176	28.9828	-2.16	0.2	-9.7	0.01		
DLPA	82.8179	28.9837	-3.06	0.01	-9.28	0.01	5.53	0.1
PYUT	82.9867	28.1013	-0.75	0.01	-1.16	0.01	0.56	0.1
BRW0	83.418	27.5073	-0.01	0.1	0.5	0.1		
TANO	83.5538	27.8738	-0.25	0.1	-0.15	0.1		
KLDN	83.6033	27.7668	-1.09	0.01	0.23	0.01	1.78	0.1
GANS	83.6426	28.599	-0.69	0.3	-8.13	0.2		
TUKO	83.6448	28.7099	-1.41	0.4	-8.46	0.4		
JALT	83.6583	28.5078	-1.02	0.2	-7.12	0.2		
JOM0	83.7179	28.7807	-0.66	0.1	-9.49	0.01		
JMSM	83.7433	28.8053	-1.99	0.01	-8.81	0.01	4.81	0.1
DNSG	83.7635	28.3451	-1.64	0.1	-6.41	0.1	4.71	0.3
BELT	83.8257	27.4574	-1.65	0.01	1.44	0.1	-0.28	0.2
SRNK	83.9358	28.2602	-1.71	0.01	-2.61	0.01	3.29	0.1
POKO	83.9777	28.199	0.41	0.5	-2.84	0.5		
PKRO	83.9817	28.1998	-0.47	0.2	-2.96	0.2		
KAWA	84.1299	27.648	-1	0.01	-0.25	0.01	0.76	0.2
DMAU	84.2652	27.9733	-0.89	0.01	-0.85	0.01	1.03	0.1
BES0	84.3734	28.229	3.59	0.2	-2.73	0.2		
BESI	84.3797	28.2286	-1.78	0.01	-3.6	0.01	3.17	0.1
CTWN	84.3853	27.6682	-0.58	0.1	-1.43	0.1	1.27	0.3
GHER	84.4097	28.3746	-2.57	0.2	-6.6	0.1		
BHAR	84.4296	27.6778	0.09	0.1	0.13	0.1		
LMJG	84.5734	28.1741	-1.25	0.1	-6.26	0.1		
SIM4	84.9852	27.1656	-0.26	0.3	0.06	0.3	-2.88	1.1
DMNO	85.1077	27.6081	-2.23	0.7	0.55	0.7		
RAM0	85.2221	28.0152	1.07	0.9	-6.31	0.9		
KKN4	85.2788	27.8007	-1.47	0.01	-1.61	0.01	2.54	0.1
KKNO	85.2791	27.8004	2.73	0.7	-0.3	0.6		
KIRT	85.2882	27.6819	1.49	0.1	2.97	0.1		
KIRT AA	85.2882	27.6819	1.49	0.1	2.96	0.2		
CHLM	85.3141	28.2072	-1.43	0.01	-7.42	0.01	6.02	0.1
PKIO	85.3982	27.5747	-0.67	0.8	-0.69	0.8		
NAGA	85.5212	27.6927	2.15	0.2	-2.03	0.2		
BAL0	85.7945	27.7454	-2.26	0.8	-0.82	0.8		
SNDL	85.7989	27.3848	-1.27	0.01	-1.45	0.01	1.02	0.1
GMB0	85.8954	27.8964	-0.7	1	-1.1	1		
RMJT	86.55	27.3051	-2.28	0.01	-3.97	0.01	4.12	0.2
RMTE	86.5971	26.9909	-2.47	0.01	-0.6	0.01	0.5	0.1
SYBC	86.7125	27.8142	-1.7	0.1	-8.84	0.1	7.97	0.5
BIRP	87.267	26.4838	1.22	0.1	-2.09	0.1		

(continued on next page)

Table 2 (continued)

Site	Longitude	Latitude	V_e	σ_e	V_n	σ_n	V_{up}	σ_{up}
BRN2	87.2722	26.5197	-0.27	0.01	-1.22	0.01	-0.76	0.1
HILE	87.3269	27.0495	1.31	0.2	-2.25	0.2		
ODRE	87.3921	26.8661	-0.26	0.01	1.05	0.01	0.54	0.1
TPLJ AA	87.7098	27.3522	-1.11	0.01	-3.27	0.01	2.64	0.1
TPLJ	87.7098	27.3522	-0.49	0.01	-3.55	0.01	4.26	0.3

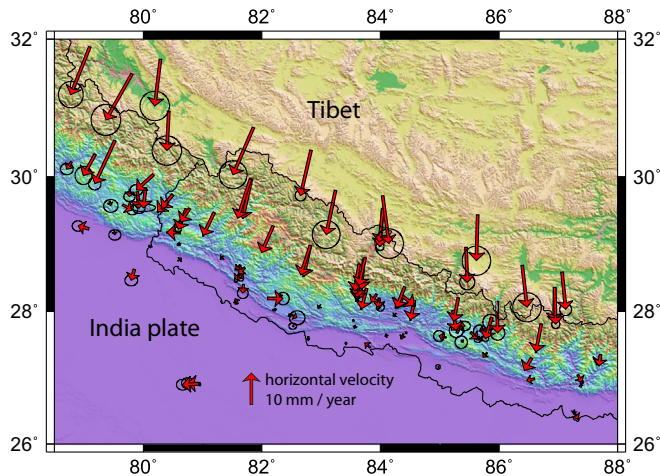


Fig. 3. Horizontal velocities expressed in the India fixed reference frame and error ellipses for a 95% confidence level. Velocities obtained with CGNSS measurements are draw with red circles in Fig. 1 and labeled in Fig. 4. (For interpretation of the references to color in this figure legend, the reader is referred to the web version of this article.)

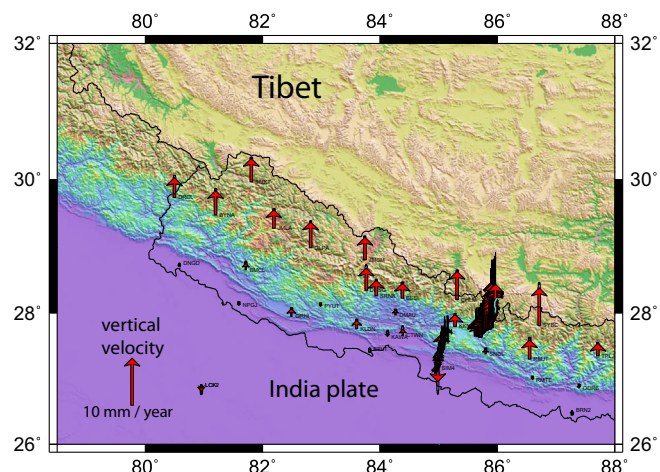


Fig. 4. Vertical velocities obtained from CGNSS stations and leveling comparison (Jackson and Bilham, 1994) and associated error for a 95% confidence level.

ramp/lower flat connection in central Nepal (Fig. 2). In Fig. 5, the location of the 25 April Gorkha earthquake indicates that this event nucleated in a locked part of the MHT and propagated eastward in the direction of a part of the MHT characterized by a lower coupling of the MHT.

In a second category of model (Fig. 8), we also added dislocations describing the Darma and the Bari Gad faults forming the eastern continuation of the Karakorum Fault as described by

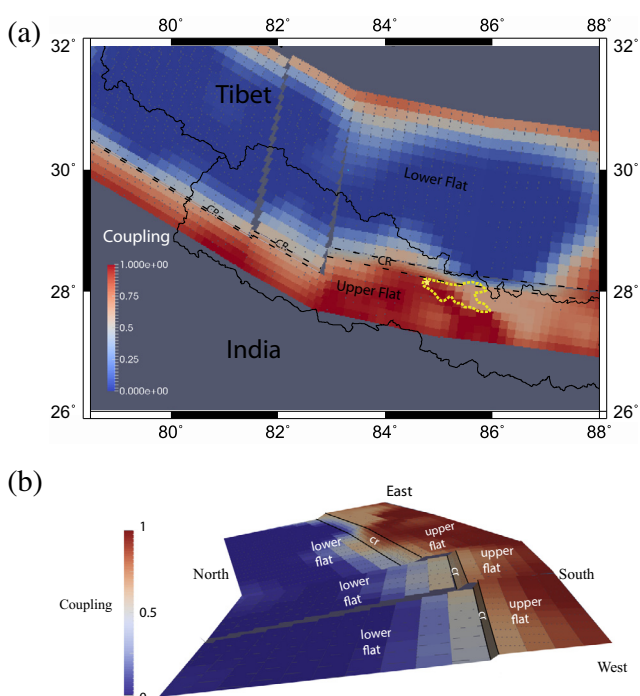


Fig. 5. Coupling along the MHT, with the system of a narrow crustal ramp in far-western Nepal, a narrower crustal ramp in western Nepal, and a wide crustal ramp in Central and Eastern Nepal. The coupling occurred north of the crustal ramp, the progressive increase in coupling illustrates a progressive brittle/ductile transition along the MHT. (a) Map view of coupling and location of the Gorkha earthquake rupture zone, CR location of the crustal ramp, and (b) perspective view of coupling along the MHT.

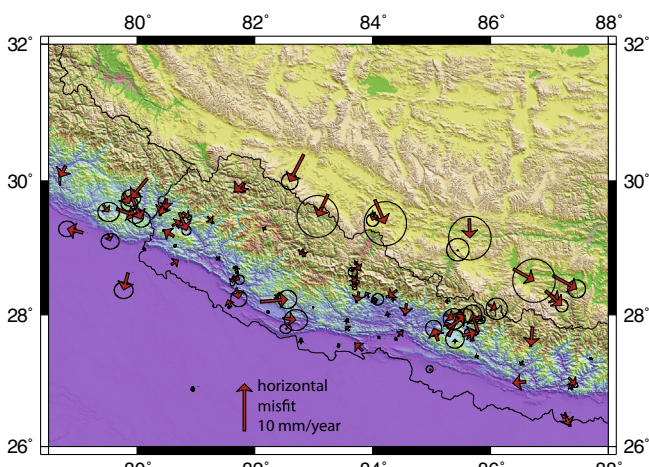


Fig. 6. Horizontal residual velocities quantifying the misfit between observed and modeled horizontal velocities with error ellipses for a 95% confidence level.

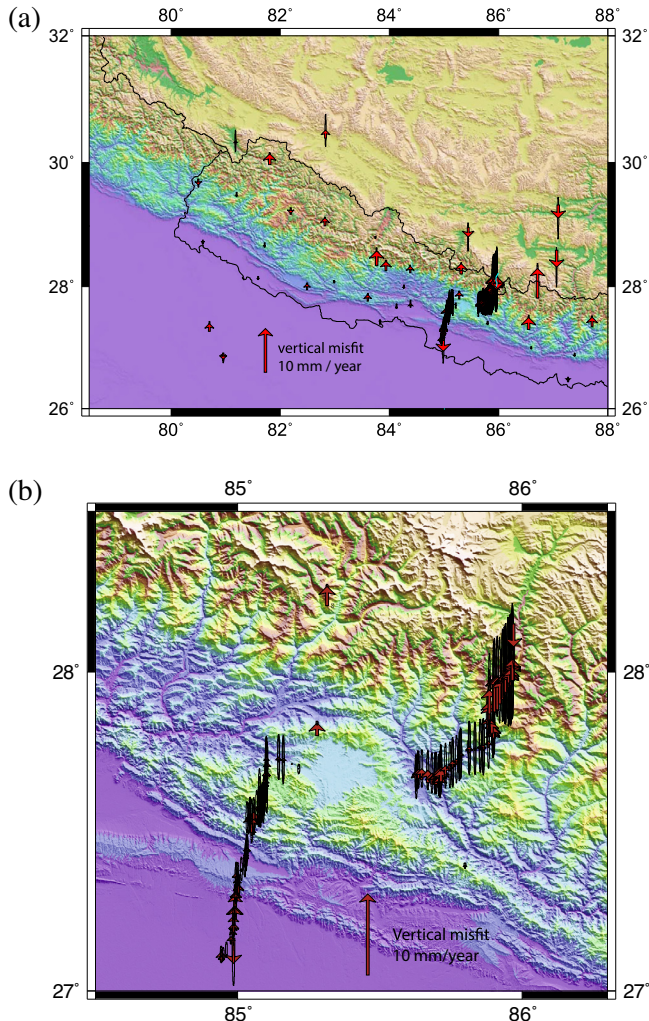


Fig. 7. Vertical residual velocities quantifying the misfit between observed and modeled horizontal velocities with error bars for a 95% confidence level.

Murphy et al. (2014) and Silver et al. (2015) (Fig. 1), to enable us to localize the strike-slip component induced by the obliquity between the shortening direction and the Main Frontal Thrust, along which the MHT emerges. For the inversion, we allowed for a strike-slip component up to 7 mm/year. This model (Fig. 8) indicates a strike-slip reaching 6.5 mm/year along the Darma-Tibrikot faults, whereas other segments are unaffected by substantial slip. Slip is only present near the surface, which implies the existence of creep along these parts of the WNFS and not at depth near the strike-slip fault/Main Himalayan Thrust connection, suggesting that the deepest parts of these faults remain locked during interseismic periods. Simulations indicated that if this fault system is active, it is linked with a band of low coupling along the MHT. The data-model correlation with the WNFS is 0.9849 whereas model without the WNFS presents a data-model correlation of 0.9905 which suggest that the introduction of the WNFS does not allow to better simulate velocities. This is also shown in Figs. 9 and 10, where residuals are larger with the model with the WNFS than with the model without the introduction of the WNFS, suggesting that this system does not play a significant role during interseismic periods. This fault system may be activated during the large Himalayan earthquakes that affect western Nepal such as the 1505 earthquake.

We can compare our results with the interseismic coupling estimation proposed by Elliott et al. (2016). The geometry for central

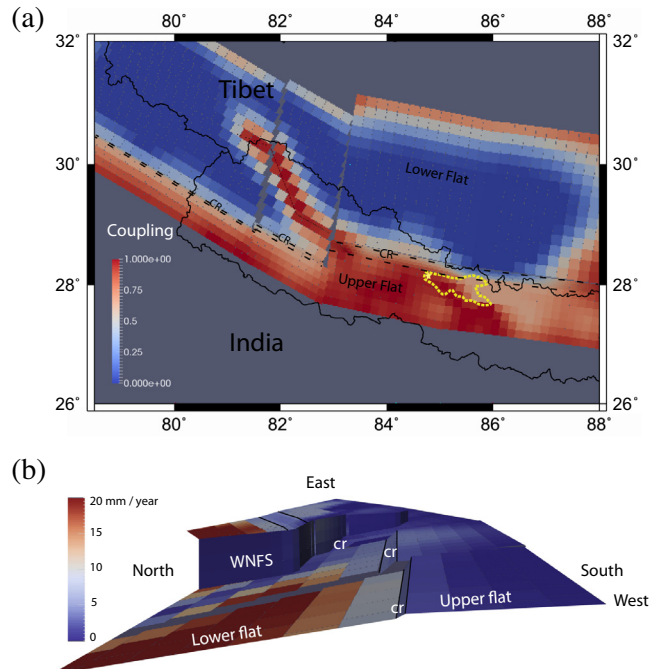


Fig. 8. Coupling along the Main Himalayan Thrust considering also the WNFS as active faults. (a) Map view of coupling along the MHT, CR location of the crustal ramp, (b) perspective view of slip distribution along the MHT and the WNFS, we draw the slip distribution and not the coupling distribution on this figure as we have no reference value for slip rate along the WNFS which do not allow the coupling computation along this fault.

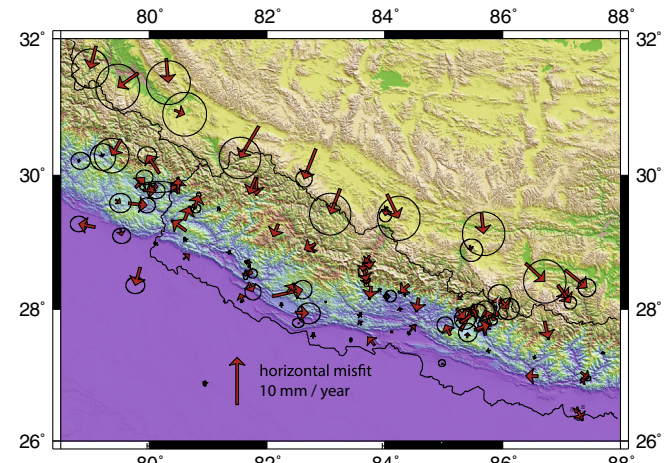


Fig. 9. Residual horizontal velocities for model 2 considering the Main Himalayan Thrust and the eastern end of Karakorum Fault active faults, with errors ellipses for a 95% confidence level.

Nepal between our model and this model differs mainly by the location of the crustal ramp, Elliott et al., 2016 propose a crustal ramp 80 km north of the Main Frontal Thrust whereas we propose a ramp localized at 100 km north of the MFT, location that has been recently confirmed by the imagery of the MHT by Duputel et al. (2016) that propose a ramp localized at 95–100 km north of the MFT. Our coupling estimates also differ, Elliott et al., 2016 proposes that the Gorkha earthquake occurs in a highly coupled segment of the MHT extending locally northward, and our preferred model (Fig. 5b) proposed a highly coupled area only in the western part of the Gorkha earthquake rupture. In other words our highly

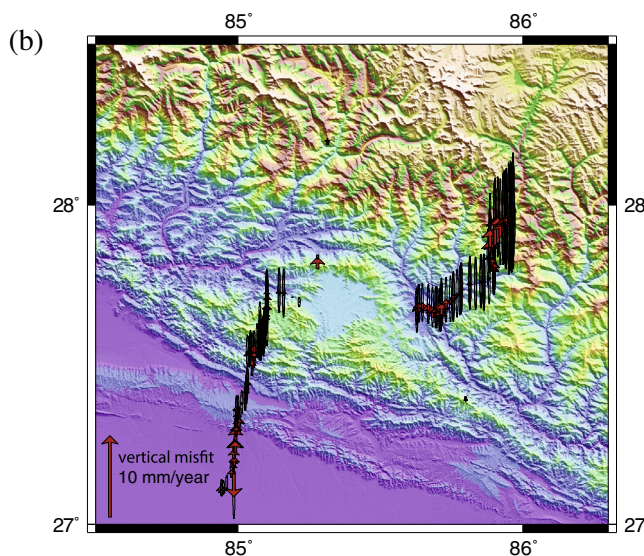
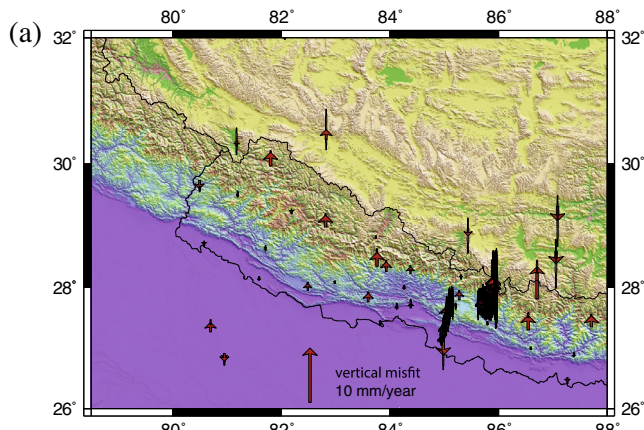


Fig. 10. Residual vertical velocities for the model considering the Main Himalayan Thrust and the eastern end of Karakorum Fault as active faults, with errors bars for a 95% confidence level.

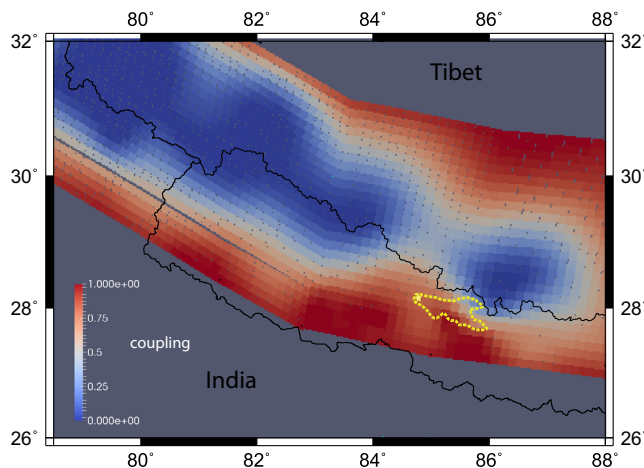


Fig. 11. Coupling along the Main Himalayan Thrust considered to be a flat dipping 7° northward.

coupled area is shifted 45–50 km westward compared to the estimation proposed by Elliott et al. (2016). These two models agree to

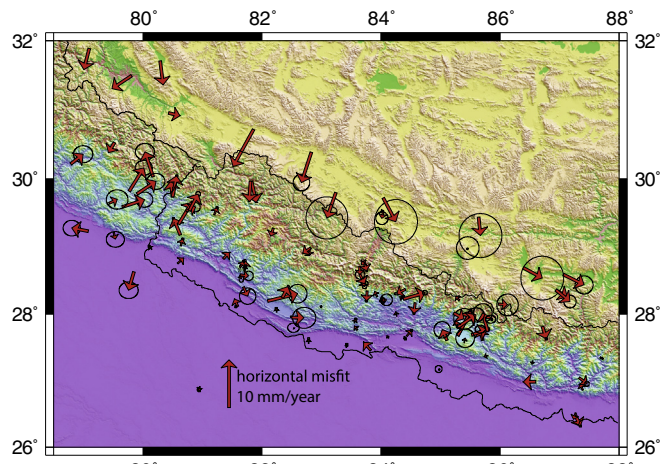


Fig. 12. Residual horizontal velocities for the model considering a flat Main Himalayan Thrust, with errors bars for a 95% confidence level.

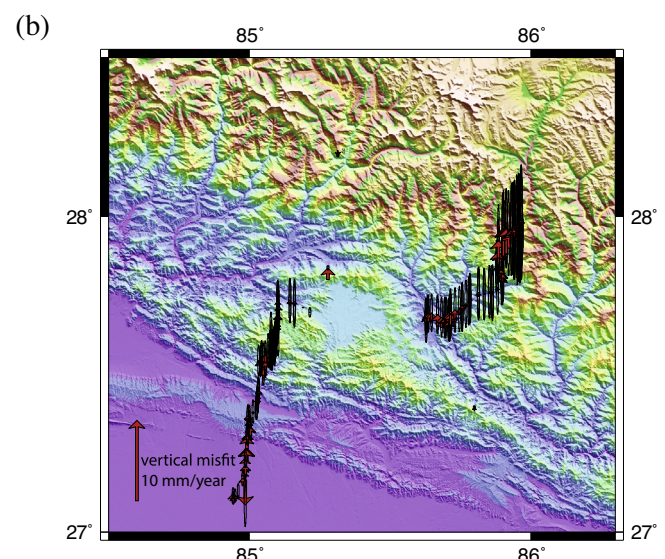
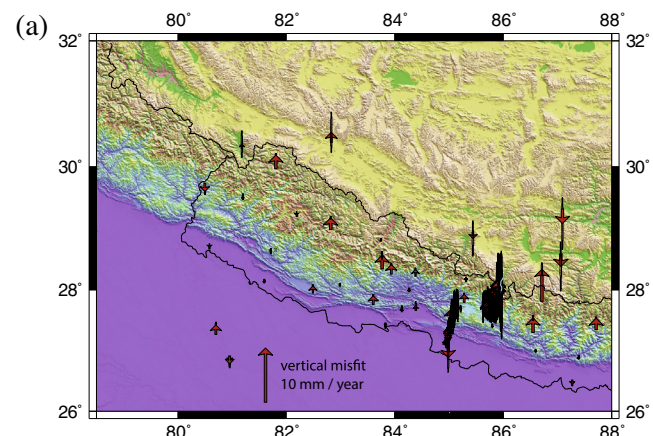


Fig. 13. Residual vertical velocities for the model considering a flat Main Himalayan Thrust, with errors bars for a 95% confidence level.

localize a less coupled area along the MHT in the Everest area in eastern Nepal where the crustal ramp seems to not be locked but affected by creep.

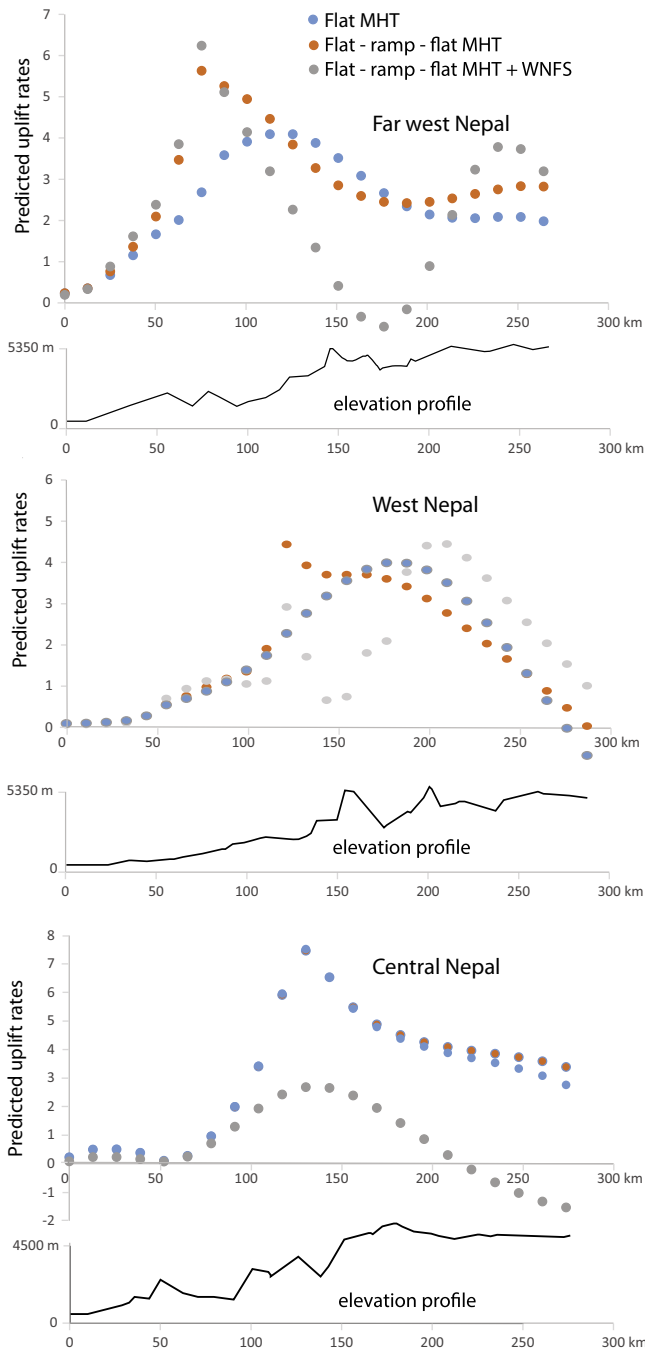


Fig. 14. Predicted vertical velocities for the far western Nepal, western Nepal and central Nepal obtained for the flat MHT hypothesis, the flat-ramp-flat MHT geometry and the flat-ramp-flat geometry with the WNFS.

6. Conclusion

We estimated horizontal and vertical velocities during the interseismic period between 1995 and the 25 April 2015 Gorkha earthquake using episodic and permanent GNSS stations and leveling comparison. We then used these velocities to estimate the coupling along the Main Himalayan Thrust by which the Indian plate underthrusts the Tibetan Plateau. Cross sections in the far-western, western, and central Himalaya allowed us to describe the geometry changes of MHT with an upper flat, a narrow or broad crustal ramp, and a lower flat beneath Tibet. Estimates of coupling along the MHT suggested a totally or partially locked upper flat, a

partially locked crustal ramp, and a lower flat the northern part of which is affected by ductile slip. Introducing the western Nepal fault system did not improve the adjustment between observed and modeled velocities. Residual uplift in the upper chain of the Himalaya suggested unmodeled phenomena such as glacial isostatic adjustment induced by the melting of Himalayan glaciers or by erosion. The Gorkha earthquake rupture began in a totally locked part of the MHT and propagated eastward through a less coupled part of the MHT. A broad zone (more than 20 km wide) located to the north of the Gorkha earthquake is partly locked and the northern boundary of the rupture is linked to the geometric flat/ramp transition rather than the rheological brittle/ductile transition.

Acknowledgments

Figures and map were prepared using Generic Mapping Tools software ([Wessel and Smith, 1995](#)) and Paraview software ([Ahrens et al., 2005](#); [Ayachit, 2015](#)). This material is based on data services provided by the UNAVCO Facility with support from the National Science Foundation (NSF) and National Aeronautics and Space Administration (NASA) under NSF Cooperative Agreement No. EAR-0735156.

References

- Ader, T., Avouac, J.P., Liu-Zeng, J., Lyon-Caen, H., Bollinger, L., Galetzka, J., Genrich, J., Thomas, M., Chanard, K., Sapkota, S., Rajaure, S., Shrestha, P., Ding, L., Flouzat, M., 2012. Convergence rate across the Nepal Himalaya and interseismic coupling on the Main Himalayan Thrust: implications. *J. Geophys. Res.* 117, B04403. <http://dx.doi.org/10.1029/2011JB009071>.
- Ahrens, J., Geveci, B., Law, C., 2005. *ParaView: An End-User Tool for Large Data Visualization*. Visualization Handbook. Elsevier, ISBN-13: 978-0123875822.
- Argand, 1924. La tectonique de l'Asie. In: *Compte Rendu Du Congrès Géologique International* (1992). Vaillant-Carmane press, Liege, Belgium, p. 104.
- Avouac, J.P., Bollinger, L., Lavé, J., Rajaure, S., Flouzat, M., 2001. Le cycle sismique en Himalaya. *C. R. Acad. Sci.* 333, 513–529.
- Ayachit, U., 2015. *The ParaView Guide: A Parallel Visualization Application*. Kitware, ISBN: 978-1930934306.
- Berger, A., Jouanne, F., Hassani, R., Mugnier, J.L., 2004. Modelling the spatial distribution of present-day deformation in Nepal: how cylindrical is the Main Himalayan Thrust in Nepal? *Geophys. J. Int.* 156, 94–114.
- Banerjee, P., Burgmann, R., Nagarajan, B., Apel, E., 2008. Intraplate deformation of the Indian subcontinent. *Geophys. Res. Lett.* 35, L18301. <http://dx.doi.org/10.1029/2008GL035468>.
- Bettinelli, P., Avouac, J.-P., Flouzat, M., Jouanne, F., Bollinger, L., Willis, P., Chitrakar, G., 2006. Plate motion of India and interseismic strain in the Nepal Himalaya from GPS and DORIS measurements. *J. Geodesy* 80, 567–589.
- Bettinelli, P., Avouac, J.-P., Flouzat, M., Bollinger, L., Ramillien, G., Rajaure, S., Sapkota, S., 2008. Seasonal variations of seismicity and geodetic strain in the Himalaya induced by surface hydrology. *Earth Planet. Sci. Lett.* 266, 332–344.
- Bilham, R., Larson, K., Freymueller, J., Idylhilm members, 1997. GPS measurements of present-day convergence across the Nepal Himalaya. *Nature* 386, 1–94 (Jouanne, F., Le Fort, P., Leturmy, P., Mugnier, J.L., Gamond, J.F., Glot, J.P., Martinod, J., Chaudury, N.L., Chitrakar, G.R., Gautam, U.P., Koirala, B.P., Pandey, M.R., Ranabhat, R., Sapkota, S.N., Shrestha, P.L., Thakury, M.C., Timilsina, U.R., Tiwari, U.R., Vidal, G., Vigny, C., Galy, A., De Voogd, B.).
- Bollinger, L., Sapkota, S.N., Tapponnier, P., Klinger, Y., Rizza, M., Van der Woerd, J., Tiwari, D.R., Pandey, R., Bitri, A., Bes de Berc, S., 2014. Estimating the return times of great Himalayan earthquakes in Eastern Nepal: evidence from the Patu and Bardibas strands of the Main Frontal Thrust. *J. Geophys. Res.* <http://dx.doi.org/10.1002/2014JB010970>.
- Chandra, U., 1992. Seismotectonics of Himalaya. *Curr. Sci.* 62, 40–72.
- Duputel, Z., Vergne, J., Rivera, L., Wittlinger, G., Farra, V., Hetényi, G., 2016. The 2015 Gorkha earthquake: a large event illuminating the Main Himalayan Thrust fault. *Geophys. Res. Lett.* 43 (2517–2525), 2016G. <http://dx.doi.org/10.1002/2016GL068083>.
- Elliott, J.R., Jolivet, R., González, P.J., Avouac, J.-P., Hollingsworth, J., Searle, M.P., Stevens, V.L., 2016. Himalayan megathrust geometry and relation to topography revealed by the Gorkha earthquake. *Nat. Geosci.* <http://dx.doi.org/10.1038/ngeo2623>.
- Fu, Y., Freymueller, J.T., 2012. Seasonal and long-term vertical deformation in the Nepal Himalaya constrained by GPS and GRACE measurements. *J. Geophys. Res.* 117, B03407. <http://dx.doi.org/10.1029/2011JB008925>.
- Galetzka, J., Avouac, J.-P., Genrich, J.F., Hudnut, K.W., 2015. Slip pulse and resonance of Kathmandu basin during the 2015 Mw 7.8 Gorkha earthquake, Nepal imaged with geodesy. *Science*, ISSN 0036-8075.
- Grandin, R., Vallée, M., Satriano, C., Lacassin, R., Klinger, Y., Simoes, M., Bollinger, L., 2015. Rupture process of the Mw = 7.9 2015 Gorkha earthquake (Nepal):

- insights into Himalayan megathrust segmentation. *Geophys. Res. Lett.* 42 (20), 8373–8382.
- Hugentobler, U., Schaer, S., Fridz, P. (Eds.), 2001. Bernese GPS Software, Version 4.2. Astronomical Institute, University of Berne.
- Jackson, M., Bilham, R., 1994. Constraints on Himalayan deformation inferred from vertical velocity fields in Nepal and Tibet. *J. Geophys. Res.* 99, 13897–13912.
- Jouanne, F., Mugnier, J.L., Pandey, M., Gamond, J.F., Le Fort, P., Serrurier, L., Vigny, C., Avouac, J.-P., 1999. Oblique convergence in the Himalayas of western Nepal deduced from preliminary results of GPS measurements. *Geophys. Res. Lett.* 26 (13), 1933–1936.
- Jouanne, F., Mugnier, J.L., Gamond, J.F., Le Fort, P., Pandey, M., Bollinger, L., Flouzat, M., Avouac, J.P., 2004. Current shortening across the Himalayas of Nepal. *Geophys. J. Int.* 157, 1–14.
- Kumar, S., Wesnousky, S.G., Rockwell, T.K., Briggs, R.W., Thakur, V.C., Jayangondaperumal, R., 2006. Paleoseismic evidence of great surface rupture earthquakes along the Indian Himalaya. *J. Geophys. Res.* 111, B03304. <http://dx.doi.org/10.1029/2004JB003309>.
- Lavé, J., Avouac, J.-P., 2000. Active folding of fluvial terraces across the Siwaliks Hills, Himalayas of central Nepal. *J. Geophys. Res.* 105, 5735–5770.
- Liang, S., Gan, W., Shen, C., Xiao, G., Liu, Chen, W., Ding, X., Zhou, D., 2013. Three-dimensional velocity field of present-day crustal motion of the Tibetan Plateau derived from GPS measurements. *J. Geophys. Res. Solid Earth* 118, 5722–5732. <http://dx.doi.org/10.1002/2013JB010503>.
- Melbourne, W.G., 1985. The case for ranging in GPS based geodetic system. Paper Presented at 1st International Symposium on Precise Positioning with the Global Positioning System, Int. Assoc. of Geod., Rockville, Md.
- Mugnier, J.L., Huyghe, P., Leturmy, P., Jouanne, F., 2004. Episodicity rates of thrust sheet motion in the Himalayas (western Nepal). In: McClay, K. (Ed.), *Thrust Tectonics and Hydrocarbon Systems*, vol. 82. AAPG Memoir, pp. 91–114.
- Mugnier, J.L., Huyghe, P., Gajurel, A., Upadhyay, B.N., Jouanne, F., 2011. Seismites in the Kathmandu valley and seismic hazard in central Himalaya. *Tectonophysics*. <http://dx.doi.org/10.1016/j.tecto.2011.05.012>.
- Mugnier, J.L., Gajurel, A., Huyghe, P., Jouanne, F., Upadhyay, B.N., 2013. Structural interpretation of the great earthquakes of the last millennium in Central Himalaya. *Earth Sci. Rev.* 127, 30–47. <http://dx.doi.org/10.1016/j.earscirev.2013.09.003>.
- Murphy, M.A., Taylor, M.H.T., Gosse, J., Silver, C.R.P., Whipp, D.M., Beaumont, C., 2014. Limit of strain partitioning in the Himalaya marked by large earthquakes in western Nepal. *Nat. Geosci.* 7, 38–42.
- Okada, Y., 1985. Surface deformation due to shear and tensile faults in a half-space. *Bull. Seismol. Soc. Am.* 75 (4), 1135–1154.
- Ostini, L., Dach, R., Meindl, M., Schaer, S., Hugentobler, U., 2008. FODITS: a new tool of the Bernese GPS software. In: Torres, J.A., Hornik, H. (Eds.), *Proceedings of EUREF 2008 Symposium*, Brussels, Belgium.
- Pagli, C., Sigmundsson, F., Lund, B., Sturkell, E., Geirsson, H., Einarsdóttir, P., Arnadóttir, T., Hreinsdóttir, S., 2007. Glacio-isostatic deformation around the Vatnajökull icecap, Iceland, induced by recent climate warming: GPS observations and finite element modeling. *J. Geophys. Res. Solid Earth* 112, B08405. <http://dx.doi.org/10.1029/2006JB004421>.
- Sapkota, S.N., Bollinger, L., Klinger, Y., Tapponnier, P., Gaudemer, Y., Tiwari, D., 2013. Primary surface ruptures of the great Himalayan earthquakes in 1934 and 1255. *Nat. Geosci.* 6, 71–76. <http://dx.doi.org/10.1038/ngeo1669>.
- Schelling, D., Arita, K., 1991. Thrust tectonics, crustal shortening, and the structure of the far-eastern Nepal Himalaya. *Tectonics* 10, 851–862.
- Shrestha, A.B., Aryal, R., 2011. Climate change in Nepal and its impact on Himalayan glaciers. *Reg. Environ. Change* 11 (1), 65–77.
- Silver, C.R.P., Murphy, M.A., Taylor, M.H., Gosse, J., Baltz, T., 2015. Neotectonics of the Western Nepal Fault System: implications for Himalayan strain-partitioning. *Tectonics*. <http://dx.doi.org/10.1002/2014TC003730>.
- Stevens, V.L., Avouac, J.-P., 2015. Interseismic coupling on the Main Himalayan Thrust. *Geophys. Res. Lett.* <http://dx.doi.org/10.1002/2015GL064845>.
- Vergne, J., Cattin, R., Avouac, J.-P., 2001. On the use of dislocations to model interseismic strain and stress build-up at intracontinental thrust faults. *Geophys. J. Int.* 147, 155–162.
- Vernant, P., Hivert, F., Chéry, J., Steer, P., Cattin, R., Rigo, A., 2013. Erosion-induced isostatic rebound triggers extension in low convergent mountain ranges. *Geology* 41, 467–470. <http://dx.doi.org/10.1130/G33942.1>.
- Wang, L., Wang, R., Roth, F., Enescu, B., Hainzl, S., Ergintav, S., 2009. Afterslip and viscoelastic relaxation following the 1999 M 7.4 Izmit earthquake from GPS measurements. *Geophys. J. Int.* 178 (3), 1220–1237.
- Wang, R., Schurr, B., Milkereit, C., Shao, Zh., Jin, M., 2011. An improved automatic scheme for empirical baseline correction of digital strong-motion records. *Bull. Seismol. Soc. Am.* 101 (5), 2029–2044. <http://dx.doi.org/10.1785/0120110039>.
- Wang, R., Parolai, S., Ge, M., Jin, M., Walter, T.R., Zschau, J., 2012. The 2011 Mw 9.0 Tohoku Earthquake: comparison of GPS and strong-motion data. *Bull. Seismol. Soc. Am.* <http://dx.doi.org/10.1785/0120110264>.
- Wessel, P., Smith, W., 1995. New version of the Generic MappingTools released. *Eos Trans. AGU* 76, 329.
- Wübbena, G., 1985. Software developments for geodetic positioning with GPS using TI4100 code and carrier measurements. Paper Presented at 1st International Symposium on Precise Positioning with the Global Positioning System, Int. Assoc. of Geod., Rockville, Md.
- Zhao, W., Nelson, K.D., Che, J., Quo, J., Lu, D., Wu, C., Liu, X., 1993. Deep seismic reflection evidence for continental underthrusting beneath southern Tibet. *Nature* 366, 555–559.